

tivated *ras*, *src*, or *HER-2*) could also result in altered cellular responses to hypoxia and could enhance the survival capacity of tumor cells under conditions of stress (22–24). Hence, one method of improving the efficacy of angiogenesis inhibitors might be to combine them with inhibitors of oncogene-mediated signal transduction, with the goal of counteracting such decreases in vascular dependence. A second method would be to combine antiangiogenic drugs with hypoxic cell cytotoxins, a new class of drugs that can overcome resistance of hypoxic cells to radiation and chemotherapy and can induce cytotoxic effects on their own (25–27). Combination bacteriolytic therapy (COBALT) could also be exploited in this manner (28). A third approach would be to use drugs such as vascular targeting agents, which can destroy existing tumor blood vessels and/or acutely disrupt blood flow (29, 30) in combination with antiangiogenic drugs that block new blood vessel formation. These various combinations also highlight the possibility that, although tumor cell variants may be able to survive under certain conditions of hypoxia, they could not do so in anoxic conditions (31).

In summary, although tumor growth and progression are angiogenesis-dependent, our results suggest that it is essential to consider the possibility that the vascular dependence of tumor cell populations may be heterogeneous, variable, and quantitative, rather than absolute and qualitative in nature. These considerations not only have important implications for the design, scheduling, and monitoring of antiangiogenic therapies in future clinical trials, but also for the interpretation of results obtained from such trials.

References and Notes

1. R. S. Kerbel, *BioEssays* **13**, 31 (1991).
2. J. Folkman, P. Hahnel, L. Hlatky, *Nature Rev. Mol. Cell. Biol.* **1**, 76 (2000).
3. T. Boehm, J. Folkman, T. Browder, M. S. O'Reilly, *Nature* **390**, 404 (1997).
4. T. Browder *et al.*, *Cancer Res.* **60**, 1878 (2000).
5. G. Klement *et al.*, *J. Clin. Invest.* **105**, R15 (2000).
6. R. A. Ezekowitz, J. B. Mulliken, J. Folkman, *N. Engl. J. Med.* **326**, 1456 (1992).
7. L. B. Kaban *et al.*, *Pediatrics* **103**, 1145 (1999).
8. R. S. Kerbel *et al.*, *Cancer Metastasis Rev.* **20**, 79 (2001).
9. E. R. Fearon, B. Vogelstein, *Cell* **61**, 759 (1990).
10. T. G. Graeber *et al.*, *Nature* **379**, 88 (1996).
11. J. Rak, R. S. Kerbel, *Cancer Metastasis Rev.* **15**, 231 (1996).
12. J. L. Yu *et al.*, *Am. J. Pathol.* **158**, 1325 (2001).
13. F. Bunz *et al.*, *Science* **282**, 1497 (1998).
14. Supplemental material is available on Science Online at [www.sciencemag.org/cgi/content/full/295/5559/1526/DC1](http://www.sciencemag.org/cgi/content/full/295/5559/1526/DC1)
15. J. L. Yu, unpublished observations.
16. Tumors were established by subcutaneous injection of a mixture of  $10^6$  *p53*<sup>+/+</sup> and  $10^6$  *p53*<sup>-/-</sup> cells. Genomic DNA was extracted from snap-frozen tumors after pulverizing the frozen tissue by using a prechilled mortar and pestle, and 15  $\mu$ g of DNA digested with Hind III, followed by Southern blotting and hybridization with a genomic *p53* probe (32). Densitometry was performed using the Image Quant system (Molecular Dynamics), and the measured per-

centage of *p53*<sup>+/+</sup> cells was determined by dividing the intensity of the 2.5-kb wild-type band by the total intensity of the wild-type plus *hyg/neo* bands (3.5/3.7 kb) (73). The actual percentage of *p53*<sup>+/+</sup> cells in a tumor was determined from a standard curve established from Fig. 2B.

17. Tumor-bearing mice were injected via the tail vein with Hoechst 33342 dye, which was allowed to circulate for 20 min before tumor removal. A single-cell suspension suitable for FACS analysis was produced by disaggregation of tumor tissue with collagenase type III, hyaluronidase, and collagenase type IV, and then resuspension in PBS. Tumor cell samples were sorted on the basis of Hoechst fluorescence intensity on an EPICS Elite V flow cytometer. Genomic DNA extracted from sorted cells was subject to polymerase chain reaction (PCR) by using the following primers: *p53* (exon 2) 5'-TGG AAG TGT CTC ATG CTG GA-3' and 5'-CAG AAC GTT GTT TTC AGG AA-3'; *p53* (exon 6) 5'-TTG CTC TTA GGT CTG GCC CC-3' and 5'-CAG ACC TCA GGC GGC TCA TA-3'. After genomic DNA extraction from sorted cells, the relative proportion of *p53*<sup>+/+</sup> cells in the proximal and distal tumor subpopulations was determined using PCR to amplify genomic sequences in exon 2 and exon 6 of the *p53* gene. The relative intensity of the exon 2 PCR product versus the exon 6 product for each DNA sample would be proportional to the relative percentage of *p53*<sup>+/+</sup> cells in each population of sorted cells. Gel band intensities were quantified using the Quantity One Gel Doc system (Bio-Rad).
18. E. M. Lord, L. Harwell, C. J. Koch, *Cancer Res.* **53**, 5721 (1993).

19. T. Waldman, K. W. Kinzler, B. Vogelstein, *Cancer Res.* **55**, 5187 (1995).
20. P. Carmeliet *et al.*, *Nature* **394**, 485 (1998).
21. N. Akakura *et al.*, *Cancer Res.* **61**, 6548 (2001).
22. G. L. Semenza, *Crit. Rev. Biochem. Mol. Biol.* **35**, 71 (2000).
23. J. Rak, J. Filmus, R. S. Kerbel, *Eur. J. Cancer* **32A**, 2438 (1996).
24. M. V. Blagosklonny, *Int. J. Oncol.* **19**, 257 (2001).
25. J. M. Brown, *Drug Resist. Updat.* **3**, 7 (2000).
26. W. A. Denny, W. R. Wilson, *Expert. Opin. Invest. Drugs* **9**, 2889 (2000).
27. S. Masunaga *et al.*, *Int. J. Radiat. Oncol. Biol. Phys.* **47**, 799 (2000).
28. L. H. Dang, C. Bettgegowda, D. L. Huso, K. W. Kinzler, B. Vogelstein, *Proc. Natl. Acad. Sci. U.S.A.* **98**, 15155 (2001).
29. J. Griggs, J. C. Metcalfe, R. Hesketh, *Lancet Oncol.* **2**, 82 (2001).
30. D. J. Chaplin, G. R. Pettit, S. A. Hill, *Anticancer Res.* **19**, 189 (1999).
31. R. S. Kerbel, J. Folkman, *Nature Rev. Cancer*, in press.
32. We thank B. Vogelstein for the HCT116 cell lines and the genomic *p53* probe; S. Green, A. Viloria-Petit, and B. Mayer for animal care assistance; and L. Woodcock and C. Cheng for excellent secretarial assistance. Supported primarily by NIH grant CA-41233 (R.S.K.), a Canadian Institutes of Health Research doctoral research award (J.L.Y.), and separate National Cancer Institute of Canada grants to B.L.C. and J.R.

26 November 2001; accepted 16 January 2002

## Transcriptional Regulation of Cortical Neuron Migration by POU Domain Factors

Robert J. McEvelly,\* Marcela Ortiz de Diaz, Marcus D. Schonemann, Farideh Hooshmand, Michael G. Rosenfeld\*

The identification of pathways mediated by the kinase Cdk5 and the ligand reelin has provided a conceptual framework for exploring the molecular mechanisms underlying proper lamination of the developing mammalian cerebral cortex. In this report, we identify a component of the regulation of Cdk5-mediated cortical lamination by genetic analysis of the roles of the class III POU domain transcription factors, *Brn-1* and *Brn-2*, expressed during the development of the forebrain and coexpressed in most layer II-V cortical neurons. *Brn-1* and *Brn-2* appear to critically control the initiation of radial migration, redundantly regulating the cell-autonomous expression of the p35 and p39 regulatory subunits of Cdk5 in migrating cortical neurons, with *Brn-1*<sup>(-/-)</sup>/*Brn-2*<sup>(-/-)</sup> mice exhibiting cortical inversion.

Development of the mammalian cerebral cortex involves both radial migration of postmitotic neurons arising from the dorsal telencephalon and tangential migration of inhibitory interneurons originating in the ganglionic eminence (1, 2). Analysis of murine mutations has partially defined two signaling pathways regulating radial migration of cortical neurons, one involving reelin, expressed in marginal zone Cajal-

Retzius cells, which binds the receptors for reelin and activates the downstream effector molecule mDab1 in radially migrating neurons (3–5), and the second mediated by Cdk5 and its regulatory subunits, p35 and p39 (6, 7).

To assess the potential roles of the class III POU domain transcription factors *Brn-1* and *Brn-2* (8–10) in cortex development, we examined the consequences of the deletion of the *Brn-1* (Web fig. 1, A to D) (11) and *Brn-2* (10) genomic loci, both separately and together. *Brn-1*<sup>(+/-)</sup> heterozygous mice were phenotypically normal; *Brn-1* gene-deleted mice were present at expected Mendelian ratios at birth but survived no longer than 36 hours postpartum, probably reflecting a defect in renal develop-

Howard Hughes Medical Institute, Department and School of Medicine, University of California, San Diego, 9500 Gilman Drive, La Jolla, CA 92037-0648, USA.

\*To whom correspondence should be addressed. E-mail: [rmcevelly@ucsd.edu](mailto:rmcevelly@ucsd.edu), [mrosenfeld@ucsd.edu](mailto:mrosenfeld@ucsd.edu)

REPORTS

ment affecting Henle's loop (12). Crosses of grossly normal *Brn-1*<sup>(+/-)</sup>/*Brn-2*<sup>(+/-)</sup> mice generated *Brn-1*<sup>(-/-)</sup>/*Brn-2*<sup>(-/-)</sup> mice at the expected 1/16 frequency, but they were not viable at birth.

In wild-type animals, *Brn-1* and *Brn-2* were normally expressed in the superficial cortical layers and ventricular zone of the neocortex at postpartum day 0 (P0), whereas *Brn-1* alone was expressed in the hippocampal CA1 field (Fig. 1A) (13). A high-magnification view illustrating costaining of *Brn-1* (red) and *Brn-2* (green) in midlateral, upper cortical plate demonstrates numerous *Brn-1*<sup>+</sup>/*Brn-2*<sup>+</sup> nuclei (yellow), with *Brn-1*<sup>+</sup> nuclei (red) also evident (Fig. 1A, upper right panel). As expected, *Brn-1* protein was undetected in the brain of *Brn-1*<sup>(-/-)</sup> mice, but the distribution of *Brn-2* protein expression was unaffected. Neither protein was detected in the brains of *Brn-1*<sup>(-/-)</sup>/*Brn-2*<sup>(-/-)</sup> mice (Fig. 1A). Neurons in *Brn-1*<sup>(-/-)</sup> and *Brn-1*<sup>(-/-)</sup>/*Brn-2*<sup>(-/-)</sup> mice that normally would have expressed *Brn-1* were marked by the presence of an mRNA transcript containing the 3' untranslated region of *Brn-1* (*Brn-1* 3'UT) (Web fig. 1E) (11, 13).

Although the cerebral cortex of *Brn-2*<sup>(-/-)</sup> mice is apparently normal (10), a substantial cellular disorganization was observed at embryonic day 18 (E18) in the hippocampus and adjacent transitional cortex of *Brn-1*<sup>(-/-)</sup> mice, which became progressively more severe by P1, extending throughout the rostrocaudal axis of the hippocampus (Fig. 1B and Web fig. 2A) (11). By E18, mRNA and protein for *Brn-1*, but not *Brn-2*, were normally present in the pyramidal neurons of the CA1 field and adjacent transitional cortex (Figs. 1 and 2A) (8, 9). At this stage, *Brn-1*<sup>+</sup> migrating neurons destined for the CA1 field in the wild-type brains, detected by the *Brn-1* 3'UT probe, were also prominently distributed between the ventricular zone and CA1 field (Fig. 2A). In contrast, *Brn-1* 3'UT<sup>+</sup> neurons accumulated as an ectopically positioned layer of densely packed cell bodies in the hippocampus of *Brn-1*<sup>(-/-)</sup> or *Brn-1*<sup>(-/-)</sup>/*Brn-2*<sup>(-/-)</sup> mice between the ventricular zone and the CA1 field, with little or no signal detected within the CA1 field (Fig. 2A). In adjacent sections, immunofluorescent localization of the subplate between the ectopic cell layer and CA1 field with the molecular marker chondroitin sulfate proteoglycan (CSPG) (14) demonstrates that neurons that would have normally expressed *Brn-1* protein are unable to migrate through the subplate to the CA1 field in single- and double-mutant mice (Fig. 2A and Web fig. 2B) (11). This migration defect appears limited to the hippocampus in the *Brn-1*<sup>(-/-)</sup> brains, but the combined gene deletion of both *Brn-1* and *Brn-2* resulted in the extension of this phenotype throughout the neocortex (Fig. 2B). Here, the distribution of *Brn-1*

3' UT hybridization signal was largely concentrated between the ventricular zone and subplate, rather than in the cortical plate, as observed in wild-type and *Brn-1*<sup>(-/-)</sup> brains (Fig. 2B), consistent with a requirement for both *Brn-1* and *Brn-2* in the regulation of radial migration of neurons in the neocortex.

We next used bromodeoxyuridine (BrdU) birth-dating analyses (13) to determine the specific cortical laminae in which *Brn-1*<sup>+</sup> neurons are normally located and to ascertain the relative locations of these laminae in the brains of corresponding *Brn-1*<sup>(-/-)</sup> and *Brn-1*<sup>(-/-)</sup>/*Brn-2*<sup>(-/-)</sup> littermates. Wild-type neurons labeled between E11 and E16 and analyzed between E16 and E19 revealed that a majority of cortical neurons born on E13 and thereafter express *Brn-1* protein, with virtually no colabeling of *Brn-1* and BrdU observed in neurons born at E11 and E12 (Web fig. 3, A to C) (11). Neurons born between E13 and E16 have been shown to contribute extensively to cortical layers II-V (15), suggesting that the neurons marked by the *Brn-1* 3'UT hybridization signal that accumulate beneath the subplate of *Brn-1*<sup>(-/-)</sup>/*Brn-2*<sup>(-/-)</sup> cortex represent this population of later-born neurons. This was confirmed by BrdU-labeling studies of wild-type, single- and double-mutant littermates conduct-

ed from E11 to E14, which demonstrate the location of early-born neurons in the superficial cortical plate and later-born neurons in the deeper layers of the *Brn-1*<sup>(-/-)</sup>/*Brn-2*<sup>(-/-)</sup> cortex. A representative example analyzed at P0 demonstrates an abnormal, superficial location of early-born subplate neurons, visualized by costaining of microtubule-associated protein 2A/2B (MAP2A/2B) (14) and CSPG, in *Brn-1*<sup>(-/-)</sup>/*Brn-2*<sup>(-/-)</sup> neocortex, and, in adjacent sections, a majority of later-born, E13 labeled neurons positioned below the subplate (Fig. 3A). In contrast, in both wild-type and *Brn-1*<sup>(-/-)</sup> brains, subplate neurons were located deep within the cortex, whereas the majority of E13 BrdU-labeled neurons were positioned above the subplate, in the cortical plate (Fig. 3A).

The cortical inversion displayed by layers II-V in the P0 *Brn-1*<sup>(-/-)</sup>/*Brn-2*<sup>(-/-)</sup> brain was further documented with a series of lamina-specific molecular markers. Expression of TLE3 and TLE1, specific for layers II-V and II/III, respectively (16), was detected by in situ hybridization in the deeper region of the cortex in *Brn-1*<sup>(-/-)</sup>/*Brn-2*<sup>(-/-)</sup> brain, rather than in the superficial layers, as observed in wild-type and *Brn-1*<sup>(-/-)</sup> littermates (Fig. 3A and Web fig. 3D) (11). In

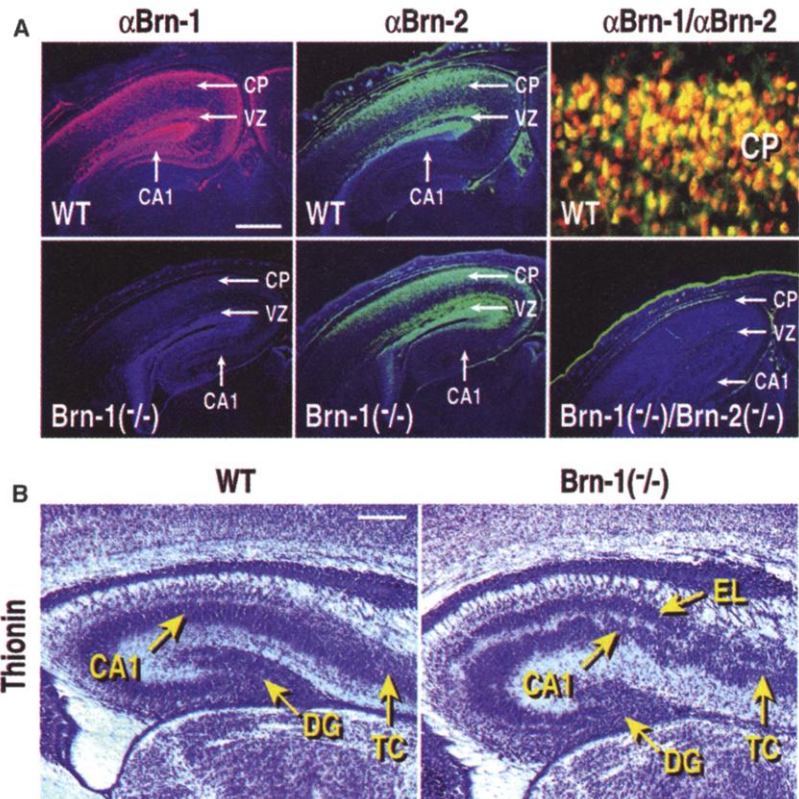


**Fig. 1.** *Brn-1/Brn-2* expression and morphology. (A) Indirect immunofluorescence detection in adjacent series of wild-type (WT), *Brn-1*<sup>(-/-)</sup>, and *Brn-1*<sup>(-/-)</sup>/*Brn-2*<sup>(-/-)</sup> P0 coronal hemisections of *Brn-1* and *Brn-2* protein, counterstained with Hoechst 33258 in low-magnification views. (B) Thionin-stained wild-type and *Brn-1*<sup>(-/-)</sup> P1 coronal sections of hippocampus. Scale bar: (A), 500 μm; (B), 125 μm. CA1, hippocampal plate; CP, cortical plate; DG, dentate gyrus; EL, ectopic cell layer; TC, transitional cortex; VZ, ventricular zone.

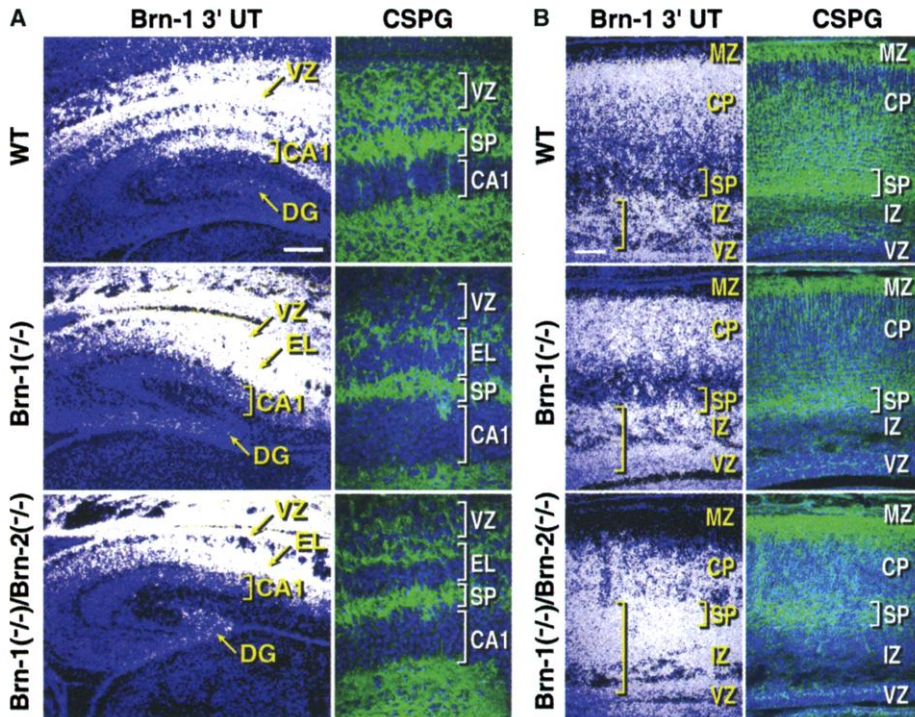
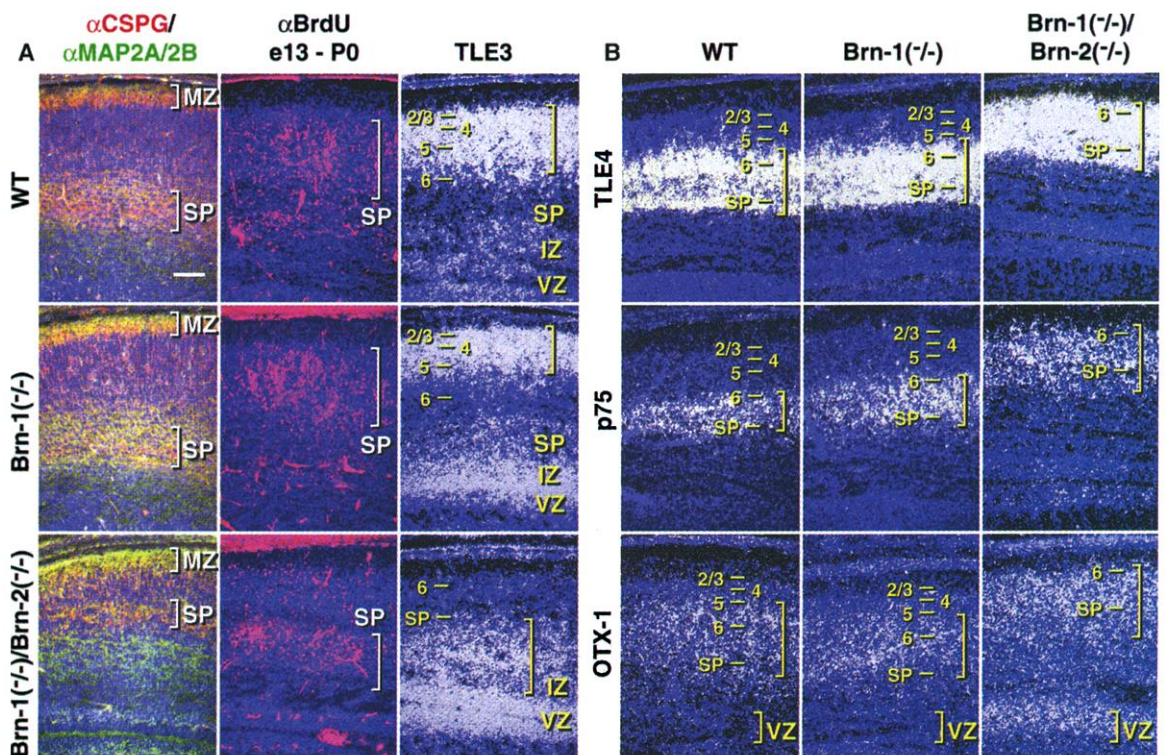


**Fig. 2.** Subplate position in wild-type and mutant brain. (A) Hippocampus and (B) neocortex of adjacent series of P0 wild type, *Brn-1*<sup>(-/-)</sup>, and *Brn-1*<sup>(-/-)</sup>/*Brn-2*<sup>(-/-)</sup> analyzed by in situ hybridization with a probe specific for *Brn-1* 3'UT (white), counterstained with Hoechst 33258 (blue), and by indirect immunofluorescence detection of CSPG (green). (A) CSPG panels represent fourfold magnified view of labeled region in adjacent in situ analyses. (B) Brackets highlight *Brn-1* 3'UT signal in VZ. Scale bar: (A and B), 250 μm. CP, cortical plate; DG, dentate gyrus; EL, ectopic layer; IZ, intermediate zone; MZ, marginal zone; SP, subplate; VZ, ventricular zone.

comparison, in situ hybridization signal specific for TLE4, OTX-1, and p75, which are expressed in cortical layer VI and in subplate neurons (16–18), was observed immediately adjacent to the marginal zone in double-mutant mice, whereas this signal was located deep in the cortical plate in wild-type and *Brn-1*<sup>(-/-)</sup> brain (Fig. 3B). Distribution patterns of two additional markers further reflected abnormal organization of cortical lamination in *Brn-1*<sup>(-/-)</sup>/*Brn-2*<sup>(-/-)</sup> brain. The expression of EphA4 (19), which was ordinarily observed as two distinct layers corresponding to layers II/III and V/VI in wild-type and *Brn-1*<sup>(-/-)</sup> brains (Web fig. 3D) (11), was altered in the *Brn-1*<sup>(-/-)</sup>/*Brn-2*<sup>(-/-)</sup>, with only one layer of signal observed in the cortical plate. Layer IV neurons, identified by the expression of ROR-β (18), were also disorganized and failed to form a cohesive layer in the upper cortical plate in *Brn-1*<sup>(-/-)</sup>/*Brn-2*<sup>(-/-)</sup> cortex (Web fig. 3D) (11). No differences in apoptotic cell death between wild-type and mutant cortex were detected by terminal deoxynucleotidyl transferase-mediated deoxyuridine triphosphate nick-end labeling (TUNEL) assay (12, 13).

Thus, *Brn-1* and *Brn-2* together are required for cell-autonomous control of radial migration in neurons of cortical layers II–V. By comparison, layer VI neurons migrated into the preplate in the *Brn-1*<sup>(-/-)</sup>/*Brn-2*<sup>(-/-)</sup> brain, splitting this structure to form

**Fig. 3.** Cell birth date and molecular marker analyses. (A and B) Indirect immunofluorescent detection of BrdU-labeled cells, CSPG and MAP2A/2B (A), and in situ hybridization serial analyses of molecular markers TLE3 (A) and TLE4, p75, and OTX-1 (B) in midlateral cerebral cortex of wild-type, *Brn-1*<sup>(-/-)</sup>, and *Brn-1*<sup>(-/-)</sup>/*Brn-2*<sup>(-/-)</sup> brain, counterstained with Hoechst 33258. The brackets in (A), illustrating BrdU-labeled neurons or TLE3-specific signal, highlight concentrations of labeled cells or in situ signal, respectively, located above the subplate (SP) in wild-type and *Brn-1*<sup>(-/-)</sup> cortex and below the SP in *Brn-1*<sup>(-/-)</sup>/*Brn-2*<sup>(-/-)</sup> cortex. The brackets in (B) illustrate in situ hybridization signal in deeper layers of cortex in wild type and *Brn-1*<sup>(-/-)</sup> and in superficial cortical layers in *Brn-1*<sup>(-/-)</sup>/*Brn-2*<sup>(-/-)</sup> brains. Scale bar: (A and B), 100 μm. 2 to 6 are the cortical layers.



REPORTS

both the marginal zone and subplate structures, indicating that these early-born neurons, in which we did not detect Brn-1 and Brn-2 expression, remain capable of normal radial migration. The inversion of cortical layers II-V observed in the *Brn-1*<sup>(-/-)</sup>/*Brn-2*<sup>(-/-)</sup> brain was similar to the migration defects reported in the gene deletions of *CDK5/p35/p39* (6, 7), whereas the phenotype reported for genetic disruption of elements of the reelin pathway (3-5) involved cortical inversion of layers II-VI.

We next examined the possibility that Brn-1 and Brn-2 might transcriptionally regulate components of these pathways. In situ hybridization analyses at E18 of elements of the reelin pathway (Web fig. 4A) (11) and immunohistochemical analysis of CDK5 expression (12) did not reveal deficiencies in the expression of these genes that are likely to be responsible for the observed phenotypes in the single or double gene-deleted mice. In contrast, in situ hybridization analyses demonstrated the expression of p35 to be markedly decreased, and that of p39 to be nearly absent, in the cortex of *Brn-1*<sup>(-/-)</sup>/*Brn-2*<sup>(-/-)</sup> double-mutant mice, although the relative cellular densities assessed by thionin

staining were similar (Fig. 4A and Web fig. 4A) (11). The expression of p35 and p39 mRNA was also nearly absent in the hippocampal CA1 fields of *Brn-1*<sup>(-/-)</sup> and *Brn-1*<sup>(-/-)</sup>/*Brn-2*<sup>(-/-)</sup> brain when compared with wild-type hippocampus (Fig. 4A). p39 and p35 remained expressed in areas where neither Brn-1 nor Brn-2 is normally expressed, including the hippocampal CA3 field of both mutant mice strains (Fig. 4A). The expression of p35 was also markedly reduced, to background levels, in the mitral cells of the *Brn-1*<sup>(-/-)</sup>/*Brn-2*<sup>(-/-)</sup> olfactory bulb (Web fig. 4B) (11), which normally express Brn-1 and Brn-2 (8, 9), and can be visualized here by the expression of reelin mRNA (20).

Inspection of 5' and 3' sequences flanking both the *p35* and *p39* genes revealed a number of consensus Brn-1 and Brn-2 DNA-binding sites (Web fig. 4C) (11) (21). Brn-1 and Brn-2 were each capable of activating transcription in transient cotransfection assays (10) >10-fold on representative examples of these response elements, and both Brn-1 and Brn-2 activated transcription three- to fourfold from the 285-base pair 5' flanking region of the *p39* gene that encompasses two Brn-1/Brn-2 consensus bind-

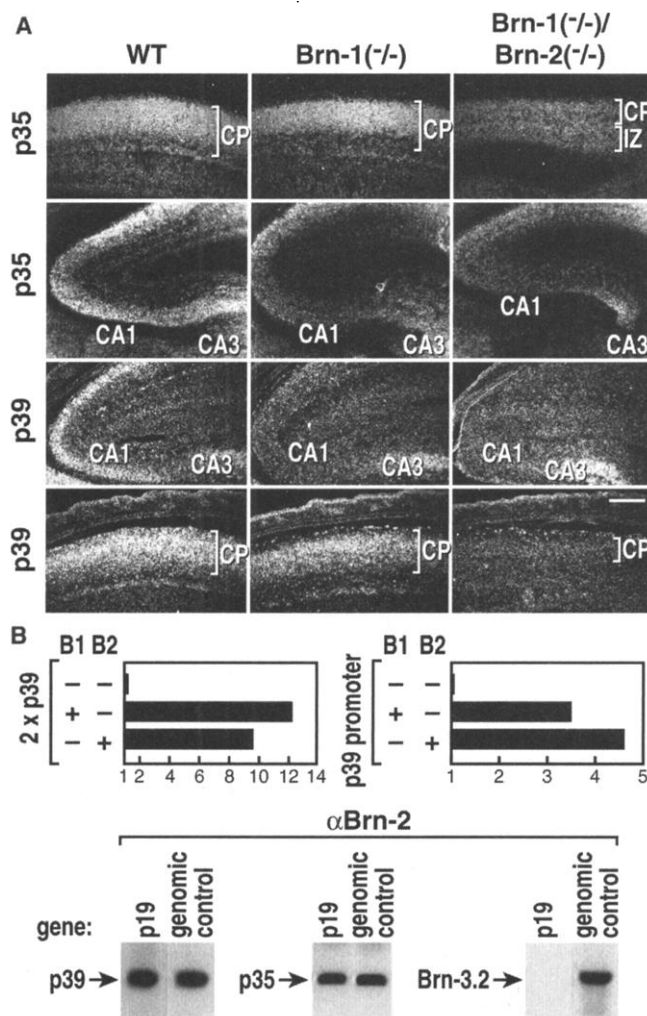
ing sites (Fig. 4B). We analyzed potential occupancy of these sites in the P19 cell line, which expresses endogenous Brn-2 protein (12, 22), by chromatin immunoprecipitation (Fig. 4B) (23, 24), finding that Brn-2 was specifically bound to both the *p35* and the *p39* regulatory regions, whereas amplification with oligomers specific for unrelated genes, such as *Brn-3.2*, failed to yield a polymerase chain reaction (PCR) product, although all pairs of oligomers amplified DNA product with equivalent ranges of sensitivity (Fig. 4B).

Additional phenotypes consistent with deficient CDK5 kinase activity (6, 7) were observed in the *Brn-1*<sup>(-/-)</sup>/*Brn-2*<sup>(-/-)</sup> cortex. One hundred sixty-kilodalton neurofilament and phosphorylated 200-kD neurofilament were not detected in axonal bundles in either *Brn-1*<sup>(-/-)</sup> or *Brn-1*<sup>(-/-)</sup>/*Brn-2*<sup>(-/-)</sup> hippocampus, although phosphorylated 200-kD neurofilament was abundant in cell bodies in the CA1 fields of these brains (Web fig. 4D) (11) (12). Abnormalities in axonal outgrowth and projection were also observed associated with the *Brn-1*<sup>(-/-)</sup>/*Brn-2*<sup>(-/-)</sup> forebrain, as well as abnormalities in migration in other regions of the CNS, including a failure of normal olfactory bulb and cerebellar development (25).

The identification of a substantial population of Brn-1<sup>+</sup>, Brn-2<sup>-</sup> cortical neurons (Fig. 1A) raised the possibility that the deletion of *Brn-1* alone might result in a partial disruption of cortical migration. Indeed, the reduced distribution of TLE3-specific signal in the cortical plate, together with decreased thickness of layer II/III EphA4 staining, and a more superficial position of ROR-β<sup>+</sup> expression in *Brn-1*<sup>(-/-)</sup> cortex, suggest a partial defect in the radial migration of a subset of neurons in cortical layers II/III (Fig. 3B and Web fig. 3D) (11). In accord with this interpretation, BrdU-labeled neurons demonstrate reduced numbers of E14 labeled neurons in the upper cortex at E17 in *Brn-1*<sup>(-/-)</sup> brain but do not reveal a gross cortical inversion within the earlier-generated neurons (Fig. 5A and Web fig. 5A) (11).

Also consistent with a reduced layer II/III migration, E12 and E13 BrdU-labeled neurons analyzed at P0 distributed in more superficial positions in *Brn-1*<sup>(-/-)</sup> cortex than in comparable wild-type regions (Web fig. 5B) (11), as did Lhx-6<sup>+</sup> and Dlx-2<sup>+</sup> interneurons (Web fig. 5D) (11) (2). Furthermore, although layer V neurons expressing Tst-1/Oct-6/SCIP (Tst-1) (8, 9) were distributed similarly in the upper cortical plate of E18 *Brn-1*<sup>(-/-)</sup> and wild-type cortex (Web fig. 5C) (11), by P1, Tst-1<sup>+</sup> neurons remained in a dorsal position in *Brn-1*<sup>(-/-)</sup> brains, partially extending into the marginal zone, rather than deeper in the cortical plate, as observed in the wild-type cortex (Fig. 5B). Because analysis of wild-type cortex revealed colocalization of Brn-1 with Tst-1 in layer V cortical neurons (Fig. 5C), both the

**Fig. 4.** p35 and p39 expression and regulation. (A) p35 and p39 expression in E18 wild type, *Brn-1*<sup>(-/-)</sup>, and *Brn-1*<sup>(-/-)</sup>/*Brn-2*<sup>(-/-)</sup> midsagittal cortex and hippocampus. Scale bar: 250 μm. (B) Transient cotransfection assay analyses of Brn-1 and Brn-2 expression plasmids with reporter plasmids containing 2x response elements or 285 base pairs of *p39* 5' flanking sequence. PCR-mediated detection of *p35* and *p39* 5' flanking sequences in αBrn-2-immunoprecipitated chromatin prepared from Brn-2-expressing p19 cells.



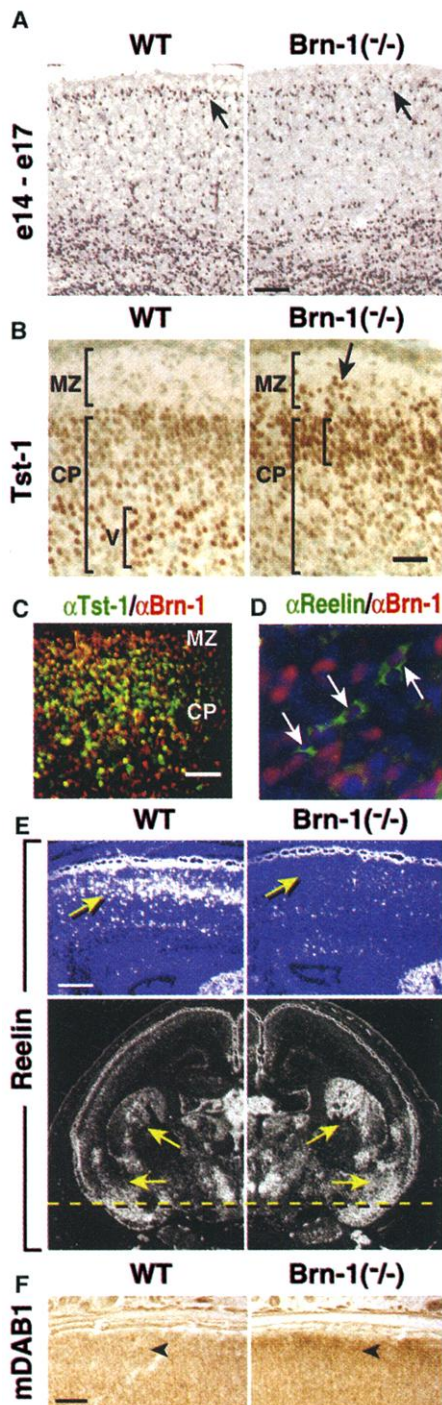


**Fig. 5.** Cortical migration defects in *Brn-1*<sup>-/-</sup> brain. (A and B) BrdU-labeled (A) and immunostaining of Tst-1<sup>+</sup> (B) neurons in midlateral cortical sections of wild-type and *Brn-1*<sup>-/-</sup> brains. (C and D) Indirect immunofluorescent colocalization of Brn-1 and Tst-1 (C) or reelin (D) in wild-type P0 midlateral coronal cortex. (E) Reelin-specific in situ hybridization signal in high and low magnifications of P0 wild-type and *Brn-1*<sup>-/-</sup> coronal cortex; arrows in low-magnification view of *Brn-1*<sup>-/-</sup> indicate increased reelin expression in basal ganglia relative to wild type. (F) Immunoperoxidase detection of mDab1 expression in midlateral coronal wild-type P1 *Brn-1*<sup>-/-</sup> cortex. Scale bars: (B), 40 μm; (C), 50 μm; (A), 100 μm; (F), 125 μm; and (E), 250 μm.

observed superficial location of Tst-1 neurons in *Brn-1*<sup>-/-</sup> cortex and the reduced migration of layer II/III neurons might reflect influences of a Brn-1-dependent, cell-autonomous mechanism analogous to that described in the *Brn-1*<sup>-/-</sup>/*Brn-2*<sup>-/-</sup> cortex.

Unexpectedly, the expression of reelin in a subpopulation of cortical plate neurons that colocalize with Brn-1 at P0 (Fig. 5D), and reportedly with markers of inhibitory interneurons in postnatal brain (20), was absent in the *Brn-1*<sup>-/-</sup> cortex, whereas reelin expression was unaffected in Cajal-Retzius neurons and even increased in basal ganglia areas (Fig. 5E), where Brn-1 expression is also normally observed (8, 9, 12). Potential roles, if any, for these Brn-1<sup>+</sup>, reelin-secreting neurons in cortical development remain to be defined, but we reproducibly found a detectable increase in mDab1-specific immunohistochemical staining in the *Brn-1*<sup>-/-</sup> in the neocortical plate (Fig. 5F), consistent with the observation that the intracellular levels of mDab1 protein increase in the absence of reelin signaling (14).

Together, these studies link Brn-1 and Brn-2 to the regulation of radial migration of layers II-V, at least in part, through regulation of the p39/p35 regulatory components of CDK5, resulting in cortical inversion in *Brn-1*<sup>-/-</sup>/*Brn-2*<sup>-/-</sup> double gene-deleted mice and disorganized cortical lamination in *Brn-1*<sup>-/-</sup> mice, where radial migration of layers II/III is delayed.

**References and Notes**

1. P. Rakic, *Science* **183**, 425 (1974).
2. S. A. Anderson, D. D. Eisenstat, L. Shi, J. L. Rubenstein, *Science* **278**, 474 (1997).
3. D. S. Rice, T. Curran, *Annu. Rev. Neurosci.* **24**, 1005 (2001).

4. J. Herz, *Neuron* **29**, 571 (2001).
5. J. A. Cooper, B. W. Howell, *Cell* **97**, 671 (1999).
6. D. S. Smith, P. L. Greer, L. H. Tsai, *Cell Growth Differ.* **12**, 277 (2001).
7. J. Ko et al., *J. Neurosci.* **21**, 6758 (2001).
8. X. He et al., *Nature* **340**, 35 (1989).
9. G. Alvarez-Bolado, M. C. Rosenfeld, L. W. Swanson, *J. Comp. Neurol.* **355**, 237 (1995).
10. M. D. Schonemann et al., *Genes Dev.* **9**, 3122 (1995).
11. See supplementary Web material (26) for Web figs. 1 to 5.
12. R. J. McEvilly, M. G. Rosenfeld, data not shown.
13. See supplementary Web material (26) for immunodetection, in situ hybridization, BrdU cell labeling, and TUNEL methodologies.
14. D. S. Rice et al., *Development* **125**, 3719 (1998).
15. T. Takahashi, T. Goto, S. Miyama, R. S. Nowakowski, V. S. Caviness Jr., *J. Neurosci.* **19**, 10357 (1999).
16. T. Allen, C. G. Lobe, *Cell. Mol. Biol.* **45**, 687 (1999).
17. D. Acampora, P. Barone, A. Simeone, *Cereb. Cortex* **9**, 533 (1999).
18. C. Zhou et al., *Neuron* **24**, 847 (1999).
19. P. A. Leighton et al., *Nature* **410**, 174 (2001).
20. S. Alcántara et al., *J. Neurosci.* **18**, 7779 (1998).
21. P. Li et al., *Genes Dev.* **7**, 2483 (1993).
22. H. Fujii, H. Hamada, *Neuron* **11**, 1197 (1993).
23. Y. Shang, X. Hu, J. DiRenzo, M. A. Lazar, M. Brown, *Cell* **103**, 843 (2000).
24. See supplementary Web material (26) for chromatin immunoprecipitation details.
25. R. J. McEvilly, M. G. Rosenfeld, in preparation.
26. Supplementary material is available on Science Online at [www.sciencemag.org/cgi/content/full/295/5559/1528/DC1](http://www.sciencemag.org/cgi/content/full/295/5559/1528/DC1).
27. The authors thank M. Becker-André for RORB cDNA, T. Curran and D. Rice for reelin and mDab1 in situ probes; A. Goffinet for reelin antisera; B. Howell for mDab1 antisera; J. Rubenstein for Dlx-2 cDNA; A. Wynshaw-Boris for reagents; A. Ryan for Brn-1/Brn-2 antisera; and L. Erkman, O. Hermanson, and K. Scully for critical reading and discussion. We thank E. Mears and P. Myer for figure preparation and H. Taylor and M. Frazer for animal husbandry. R.J.M. was a recipient of a National Alliance for Research on Schizophrenia and Depression young investigator award; M.G.R. is an Investigator with Howard Hughes Medical Institute. This research was supported by a grant from the National Institute of Neurological Disorders and Stroke.

15 October 2001; accepted 18 January 2002

## Functional MRI of Macaque Monkeys Performing a Cognitive Set-Shifting Task

Kiyoshi Nakahara,<sup>1</sup> Toshihiro Hayashi,<sup>1,2</sup> Seiki Konishi,<sup>1</sup> Yasushi Miyashita<sup>1,3\*</sup>

Functional brain organization of macaque monkeys and humans was directly compared by functional magnetic resonance imaging. Subjects of both species performed a modified Wisconsin Card Sorting Test that required behavioral flexibility in the form of cognitive set shifting. Equivalent visual stimuli and task sequence were used for the two species. We found transient activation related to cognitive set shifting in focal regions of prefrontal cortex in both monkeys and humans. These functional homologs were located in cytoarchitecturally equivalent regions in the posterior part of ventrolateral prefrontal cortex. This comparative imaging provides insights into the evolution of cognition in primates.

The prefrontal cortex (PFC) is evolutionarily most developed in primates and supports higher cognitive functions. Macaque mon-

keys have been widely used for investigating the PFC, mainly in anatomical, electrophysiological, and lesion studies (1–5), whereas